Cellulose (2022) 29:9531–9547
https://doi.org/10.1007/s10570-022-04870-6

ORIGINAL RESEARCH

Cellulose nanocrystal-based enhancement of ultrasound microbubbles for increased tolerance of mechanical index values

Yiwei Wang · Na Li · Shaobo Duan · Ye Zhang · Yuzhou Wang · Beibei Zhang · Shanshan Ren · Lianzhong Zhang

Received: 24 November 2021 / Accepted: 10 August 2022 / Published online: 12 October 2022

Abstract Enhancements in the echo intensity and mechanical index (MI) tolerance of ideal ultrasound contrast agents (UCAs) are urgently needed to realize precise clinical ultrasound (US). Solid cellulose nanocrystals (CNCs) have the advantages of imparting strong sound wave propagation and echo intensity when irradiated by US. This study aimed to fabricate improved UCAs via CNC-modified SonoVue ultrasound microbubbles (MBs), characterize the resulting SonoVue@CNC MBs, and evaluate the performance of the SonoVue@CNC MBs in US imaging in vitro and in vivo. SonoVue@CNC MBs were successfully prepared by incorporating CNCs into SonoVue MBs via self-assembly. The SonoVue@CNC MBs were spherical in shape with mean particle sizes of (5.50 ± 1.60) μm. The CNCs were mainly distributed on the polymeric shells of the SonoVue@CNC MBs. When the MI was 0.4, the echo intensity of the SonoVue@CNC MBs was 1.5-fold greater than that of the SonoVue MBs in vitro. The CNC concentration regulated the quality of SonoVue@CNC-promoted contrast-enhanced ultrasound (CEUS) images. Enhanced US images of both the livers and kidneys of Sprague–Dawley (SD) rats showed that the CNC-loaded UCA led to a higher echo intensity than SonoVue. In CCK-8 assays using MCF-10A cells, both SonoVue@CNC MBs and CNCs exhibited weak toxicities against MCF-10A cells. Ultimately, the spherical SonoVue@CNC MBs with a uniform particle size displayed an enhanced safety profile and improved the imaging quality of US in vivo and in vitro. Next, drugs and targeting moieties will be loaded onto the SonoVue@CNC MBs via the CNCs to develop UCA-based selective ultrasonic theranostic methods.

Yiwei Wang and Na Li have contributed equally to the study.

Supplementary Information The online version contains supplementary material available at https://doi.org/10.1007/s10570-022-04870-6.

Y. Wang · N. Li · L. Zhang (✉)
Zhengzhou University People's Hospital, Zhengzhou University, Zhengzhou, China
e-mail: zlz8777@163.com

Y. Wang · N. Li · S. Duan · Y. Zhang · Y. Wang · B. Zhang · S. Ren · L. Zhang
Henan Provincial People's Hospital, Zhengzhou, China

Y. Wang · N. Li · S. Duan · Y. Zhang · Y. Wang · B. Zhang · S. Ren · L. Zhang
Henan Provincial Key Laboratory of Ultrasound Imaging and Artificial Intelligence, Henan Provincial People's Hospital, Zhengzhou, China

N. Li
Henan Institute of Medical and Pharmaceutical Sciences, Zhengzhou University, Zhengzhou, China

Graphical abstract As shown in the graphical abstract, the white bubble in the left-middle position symbolized SonoVue microbubble (MB), the green rod-like particle signified CNC nanorod. The big white bubble decorated with green rod-like nanorod next to the mouse was SonoVue@CNC MB which was successfully prepared by incorporating CNCs into SonoVue MB via self-assembly. The purple square frame on the upper left displayed CNC, SonoVue MB, SonoVue@CNC MB and their relative diagrammatic drawings. Picture (I) displayed the transmission electron microscopy results for CNCs (a) and SonoVue@CNC MBs (b, c and d) of morphological study. Picture (II) displayed the in vitro ultrasound (US) imaging of SonoVue (a) MB and SonoVue@CNC (b, c and d) MBs with different CNCs concentrations. Picture (III and IV) displayed the in vivo US imaging of SonoVue (a) and SonoVue@CNC (b, c and d) MBs with different CNCs concentrations for SD mouse liver and kidney, respectively.

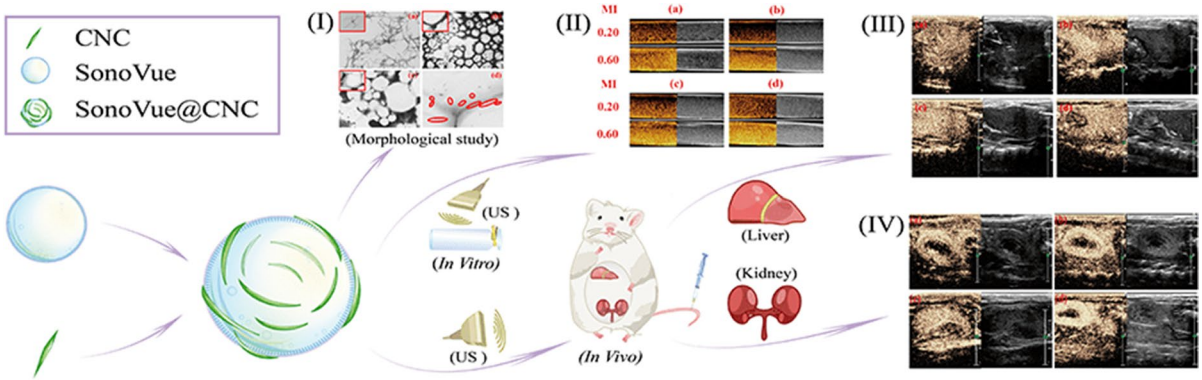

Keywords Cellulose nanocrystals (CNCs) · SonoVue · Microbubbles (MBs) · Ultrasound contrast agents (UCAs) · Mechanical index (MI)

Introduction

Cellulose nanocrystals (CNCs) are fascinating biorenewable nanoscale materials (Ates et al. 2020), which are hydrolysed via strong acids or bases from natural celluloses (Lu and Lo 2010; Pereira et al. 2020). CNCs have been extensively applied in biomedical research (Jorfi et al. 2013), such as in drug delivery systems (Trache et al. 2017), nanomedicines (Lin and Dufresne 2014; Tang et al. 2017; Sheikhi et al. 2019) and medical image (Chen et al. 2014; Liu et al. 2015; Imlimthan and Keina 2018; Sheikhi et al. 2019). Our previous studies confirmed that CNC nanoparticles could be modified by physical absorption and chemical bonding for biomedical research applications (Li et al. 2018, 2019b, 2021). In detail, CNC-based rodlike shaped nanomedicines enhanced cellular uptake and intracellular drug controlled release (Li et al. 2018). Combine with folate, CNC-based nanomedicines could realize targeted delivery and lysosomal pH-controlled drug release into the nucleus (Li et al. 2019b). Loaded with Fe_3O_4, DOTA and In, CNCs have also been used to develop new contrast agents for medical magnetic resonance imaging and SPECT/CT imaging (Chen et al. 2014; Imlimthan et al. 2019). Though solid CNCs can impart strong sound wave propagation and echo intensity when exposed to ultrasound (US) waves, there are few reports about the applications of CNCs in ultrasound contrast agents (UCAs).

US is one of the most widely used and safest modalities for clinically visualizing tissues and organs due to its high sensitivity, broad accessibility, portability, and low cost (Bez et al. 2019). Medical US imaging is based on the scattering and reflection of sound waves from the interfaces between materials and/or tissues. UCA is a liquid with small, encapsulated bubbles or droplets that very efficiently scatter US, which can improve US imaging quality and increase the diagnostic ability of US. Typically, UCAs have a shell-core structure, and thus, UCAs can be simply divided into gas-filled MBs, perfluorocarbon-filled droplets and solid-shell based UCAs.

US imaging enhancement and applications of UCAs can be affected by their size, shell materials, viscosity and density. Specifically, the particle size affects the stability and acoustic backscatter signals, the shell materials affect the stability and circulation time, and the viscosity and density affect the echo intensity. Compared to the perfluorocarbon-filled droplets and solid-shell based UCAs, the gas-filled MBs displayed the largest size and highest acoustic backscattering. The size of MBs mostly ranges between 1 and 8 μm in diameter. Therefore, gas-filled MBs have been extensively used to increase the applications of US diagnosis. However, their relatively low stability and low mechanical index (MI) tolerances have greatly limited their clinical applications. For example, sulfur hexafluoride-filled SonoVue ultrasound MBs, whose diameter is approximately 5.50 ± 1.60 μm, have been extensively used to achieve the contrast US imaging of organs. As a commercially available MB, SonoVue itself has been used to develop drug delivery systems and realize US-based therapeutic modality. SonoVue was developed for diagnostic use only, but its relatively low stability and low MI tolerance led to a short circulation time in vivo, which reduced the observation time and precision of US diagnosis and increased the operational difficulty for US doctors and the treatment cost and suffering of the patients (Lindner 2004; Thomas et al. 2019). The applications of SonoVue MBs also have thus been greatly limited.

A CNC is non-toxic, biocompatible, biodegradable and amphipathic nanoparticle. With a high Young's modulus and excellent flexibility (Cintrón et al. 2011), CNCs can maintain their size and shape during blood circulation. Moreover, CNCs have been extensively studied in many scientific fields, especially in biomedical fields. Different CNCs derived from different materials display different shapes (French and Santiago Cintrón 2013). Furthermore, the different shapes of CNCs present specific advantages for different applications. Rod-like and spherical nanoparticles and CNC nanoparticles have been shown to demonstrate different pharmacokinetic properties in vivo. Spherical nanoparticles tend to migrate with blood flow and are highly likely to be cleared (Chithrani and Chan 2007; Gratton et al. 2008; Albanese et al. 2012; Toy et al. 2014). In contrast, rod-like nanoparticles tend to move near vascular walls and can have a long circulation time, easily penetrate blood vessel gaps and accumulate in tumours (Seo et al. 2020), Indeed, rod-like CNC-based nanomedicines have exhibited long circulation times, good compatibilities with amphipathic polymers, target molecules and chemotherapeutic agents (Li et al. 2019c) (Li et al. 2021) and the improved inhibition of cancer cell proliferation (Li et al. 2018). In addition, as solid nanoparticles, CNCs possess high sound wave propagation and strong echo intensity when irradiated by US. CNCs and CNC-based nanomedicine-modified bubbles can display better echo intensities than bubbles alone under the same US irradiation (Wang et al. 2019).

We hypothesize that CNCs and CNC-based nanomedicines can be used to modify SonoVue MBs to achieve imaging-guided therapy and US-based theranostics. Moreover, CNCs, as nanodrug carriers prepared by self-assembly technology, facilitate targeted drug delivery (Li et al. 2019a) but have no imaging or cavitation properties. Therefore, the combination of CNCs and SonoVue MBs can improve the US imaging quality and the precision of US diagnosis. Nonetheless, few to no studies have explored such combinations in this context. In this study, we aimed to improve SonoVue, a commercially available UCA, by enhancing its echo intensity and MI tolerance to realize precise clinical US with an ideal UCA. Herein, we used several CNCs obtained from different origins to prepare CNC-modified SonoVue-based UCAs and evaluated the performance of SonoVue@CNCs in US imaging in vitro and in vivo. In fact, the results showed that CNCs could be successfully incorporated into SonoVue MBs, and the resulting compound showed better enhancement for in vitro and in vivo US images, with little toxicity in vitro. The CNC concentration could be used to regulate the quality of SonoVue@CNC-promoted contrast-enhanced ultrasound (CEUS) images in vitro and in vivo. CNC-modified SonoVue can also provide basic knowledge and research experience for the applications of CNC-based nanomedicines and MBs in ultrasonic theranostic systems.

Materials and methods

Materials

SonoVue MBs, which contained polymer powder (25 mg) and sulphur hexafluoride (CAS: 2551-62-4 34 mg), were purchased from Bracco Suisse (Batch

No.21A061A). Rod-like CNC freeze-dried powder (CAS No: NONE8013, Product No: C909405), TEMPO-functionalized CNCs (TEMPO-CNCs, CAS No: 9004-34-6, Product No: C916570) that were prepared by the oxidation of the rod-like CNCs and contained both hydroxyl and carboxyl groups on their surface (synthesis scheme shown in the supporting information S1), rod-like CNCs-M (CAS No: 9004-34-6, Product No: C916569) in a milky white emulsion with only hydroxyl groups on their surface (preparation scheme shown in the supporting information S1), rod-like B-CNCs (CAS No: 9004-34-6, Product No: C38724) that were hydrolysed via strong acids from bacterial cellulose, and nanolignocellulose (CN-Ls, CAS No: 9004-34-6, Product No: 102330) were purchased from ScienceK Co., Ltd. Cellulose nanowhiskers (CN-Ws, CAS No: 9004-34-6, Product No: 435244) and cellulose nanofibrils (CN-Fs, CAS No: 9004-34-6, Product No: C875077) were purchased from Northern Century (Jiangsu) Cellulose Material Co., Ltd. Rod-like amino-functionalized CNCs (CNC-NH_2) were donated by the Li laboratory at Zhengzhou University and prepared according to previously reported methods (Li et al. 2018). More detailed information on the eight types of CNCs used in this study is available in the supporting information in S1. Saline was purchased from Jiangsu Hengrui Medicine Co., Ltd. Both the MCF-10A human breast epithelial cell line (CL-0525) and DMEM(CM-0525) were kindly provided by Procell Life Science&Technology Co.,Ltd. CCK-8 reagent was purchased from Beiren Chemical Technology (Beijing) Co., Ltd. Other reagents were used as received. All chemical reagents were analytically pure.

Preparation of SonoVue@CNC MBs

All eight MB samples were simply obtained by mixing CNCs in SonoVue solution. In detail, rod-like CNC powder (25 mg) was dissolved in saline (5 mL) to form a CNC solution and sonicated for 15 min using an ultrasonic cleaning machine (KQ-250DE, Kunshan) to ensure uniform dispersion. The CNC solution (5 mg/mL) was injected into SonoVue to create CNC-modified gas-filled MBs, i.e., SonoVue@CNCs (25 mg/5 mL). Both the SonoVue MBs and SonoVue@CNCs were dropped onto a glass slide, respectively, and observed by inverted fluorescence microscopy (IFM, Olympus IX53, Japan) at × 100 magnification. Thirty bubbles were randomly selected via measurement software on the Olympus and used to calculate the MB particle size, and the mean and standard deviation (SD) were calculated. CNCs, SonoVue MBs, and SonoVue@CNCs were added dropwise onto a copper mesh for morphological analysis by transmission electron microscopy (TEM) (JEM-1400, Japan). CNC-NH_2, TEMPO-CNCs, CNCs-M, B-CNCs, CN-Ls, CN-Ws, and CN-Fs, were also used to fabricate CNC-loading SonoVue@CNC MBs via the aforementioned methods (additional details are presented in the supporting information in S2).

Physicochemical characterization

TEM and IFM were used to observe the structural and morphological characterizations of the CNCs and CNC-based SonoVue@CNC MBs. X-ray diffractometry (XRD), differential scanning calorimetry (DSC), and thermogravimetric analysis (TGA) were used to study the thermal stability and relevant physicochemical properties of the different types of CNCs and eight corresponding CNC-based SonoVue@CNC MBs. The details of each analysis are described in supporting information S2.

Cell culture

MCF-10A cells were cultured in DMEM supplemented with 10% foetal bovine serum (FBS, HyClone, Logan), streptomycin (100 μg/mL), and penicillin (100 g/mL). All cells were incubated at 37 °C under 5% CO_2.

Toxicity in MCF-10A cells

The cytotoxicities of SonoVue, the rod-like CNC freeze-dried powder (CAS No: NONE8013, Product No: C909405) and CNC-based SonoVue@CNCs were evaluated by CCK-8 assays against MCF-10A cells. MCF-10A cells (5×10^3 cells) were plated in 96-well plates with culture medium (200 μL in each well). The cells were incubated at 37 °C under 5% CO, and the supernatant was discarder 24 h later. The cells were washed three times with PBS (200 μL).

For the SonoVue@CNC groups, 200 µL of culture medium containing SonoVue@CNCs with different CNC concentrations was added (the CNC concentrations were 0.07 mg/mL, 0.15 mg/mL, 0.31 mg/mL, 0.62 mg/mL, 1.25 mg/mL, and 2.5 mg/mL). Six replicate wells were used for each concentration. For the CNC groups, 200 µL of the complete medium containing different concentrations of CNCs (according to our previous study (Li et al. 2018), CNC concentrations of 0.07 mg/mL, 0.15 mg/mL, 0.31 mg/mL, 0.62 mg/mL, 1.25 mg/mL, and 2.5 mg/mL were chosen) was used to replace the old medium. Then, all 96-well plates were incubated for 6 h, 12 h, and 24 h. Next, the culture was discarded, and the cells were washed three times with PBS (200 µL). Finally, 100 µL of complete medium containing 10 µL of CCK-8 reagent was added, and the plates were incubated for another 2 h. A microplate reader (Bio-Tek, USA) was used to determine the OD value of each well at 450 nm, and the survival rate of the cells was calculated.

In vitro *ultrasound imaging study*

For the in vitro US imaging study, 1 mL of SonoVue (5 mg/mL) and different concentrations of the SonoVue@CNC types that were prepared by the same method as described above (the concentrations of CNCs were 12.5 mg/mL, 25 mg/mL and 50 mg/mL, with an equivalent SonoVue concentration of 5 mg/mL) were injected into the rubber head of a dropper. CEUS and B-mode US were carried out using a HI VISION Ascendus US diagnostic system (HITACHI, Japan) equipped with an EUP-L74M Linear array transducer (5–13 MHz) at different MIs (0.08, 0.20, 0.40, 0.60, and 0.80). The MI is used to test the stability and tolerance for US irradiation, which also can indicate the potential of ultrasonic mechanical effects to cause biological effects. Ultrapure water was used as a control.

In vivo *ultrasound imaging study*

Healthy female SD rats were selected from the Biotechnology Co. SPF (Beijing), with a body weight of about 120 g, aged 5 weeks and SPF grade. Female SD rats were anesthetised by sodium pentobarbital (40 mg/kg) via intraperitoneal injection. The SD rats were sacrificed by the mercy killing method at the end of the experiments.

All eight types of SonoVue@CNCs were used for in vivo US imaging. Twenty-four healthy SD rats were randomly divided into four groups, with six rats each. Three groups were injected with 200 µL of SonoVue@CNCs with different CNC concentrations (6.4 mg/mL, 13.2 mg/mL, and 26 mg/mL) via the tail vein. The fourth group of controls were also injected with 200 µL of SonoVue with an equivalent concentration of 5 mg/mL via the tail vein. Forty-two healthy SD rats were randomly divided into seven groups with six rats each that were used for in vivo US imaging with the other seven types of SonoVue@CNCs (6.4 mg/mL) through the same method as stated above. Then, an EPIQ7 US diagnostic system (Philips, USA) equipped with a L12-5 Linear array transducer (5–12 MHz) was used to perform the CEUS and B-mode US imaging of the livers and kidneys at an MI of 0.19. A high MI can indicate the high potential of ultrasonic mechanical effects to cause biological effects. US irradiation with an MI of 0.19 could produce an ideal US echo intensity without causing too many biological side effects. To expound upon the changes in echo intensity, the livers were imaged 10 s after intravenous injection, and the kidneys were observed at 0, 5, and 10 s after the injection. The echo intensity of the livers and kidneys in SD mice imaged with different UCAs (SonoVue@CNCs and SonoVue) was quantitatively analysed with quantitative analytical software corresponding to the diagnostic colour Doppler US system. The intensity values in the ROIs were also analysed.

Statistical analysis

The echo intensity in the region of interest (ROI), which was a circle with a diameter of 1.0 cm, was quantitatively analysed by the data analysis software QLAB10. Statistical analyses were performed using SPSS 25.0. Measurement data are expressed as $\bar{x} \pm s$. The means of multiple groups were compared using one-way analysis of variance. Intergroup comparisons were performed using the t test. Statistical significance was set at $P < 0.05$.

Results and discussion

Characterization of CNCs

The eight compounds used in this text, CNCs, CNC-NH2, TEMPO-CNCs, CNCs-M, CN-Ls, B-CNCs, CN-Ws and CN-Fs, were all nanocelluloses with crystalline regions of cellulose that were observed as nanoscale needle-like particles (Sheikhi et al. 2019). Nanocelluloses display high Young's moduli and excellent flexibilities, which indicates CNCs can maintain their size and shape during blood circulation. Solid nanocelluloses impart strong sound wave propagation and echo intensity when exposed to US waves. Rod-like CNCs tend to move near vascular walls are highly likely to avoid macrophage endocytosis, resulting in a relatively long circulation time in vivo and enhanced accumulation in tumour tissues. As such, the incorporation of CNCs into an existing UCA, such as SonoVue MBs, could offer improved US imaging and diagnosis. First, the eight types of CNCs used to create SonoVue@CNC MBs were characterized by TEM as shown in Fig. 1.

As shown in Fig. 1, CNCs (a) were rod-like nanoparticles, whose mean aspect ratio was 10.26 ± 1.06 calculated by ImageJ software. Comparing with related literature, CNCs (a) showed typical TEM images of cellulose I (Guo et al. 2016; French and Santiago Cintrón 2013; French 2014). All eight types of nanocellulose: CNCs (a), CNC-NH_2 (b), TEMPO-CNCs (c), CNCs-M (d), CN-Ls (e), B-CNCs (f), CN-Ws (g) and CN-Fs (h), were observed by TEM, which confirmed that these CNCs were all rod-like solid particles with different length-to-diameter ratios. These materials were all used to prepare SonoVue@CNC MBs.

Synthesis of SonoVue@CNC MBs

This manuscript describes the synthesis, characterization and in vitro and in vivo evaluation of eight types of CNC-modified SonoVue MBs (SonoVue@CNCs). It was found that the addition of CNCs to SonoVue MBs did not alter their spherical morphology. Additionally, SonoVue@CNCs showed improved enhancement in both in vitro imaging and rat liver and kidney imaging in vivo, with minimal cytotoxicity, and demonstrated better tolerance to increased MI values.

Morphological properties of SonoVue@CNC MBs

After characterization, the eight types of CNCs were incorporated into SonoVue MBs to create eight corresponding types of SonoVue@CNC MBs. IFM and TEM were used to observe the morphological properties of SonoVue@CNC MBs, and the results were as follow:

The morphology of the newly prepared SonoVue@CNC MBs was firstly analysed via IFM. Both the

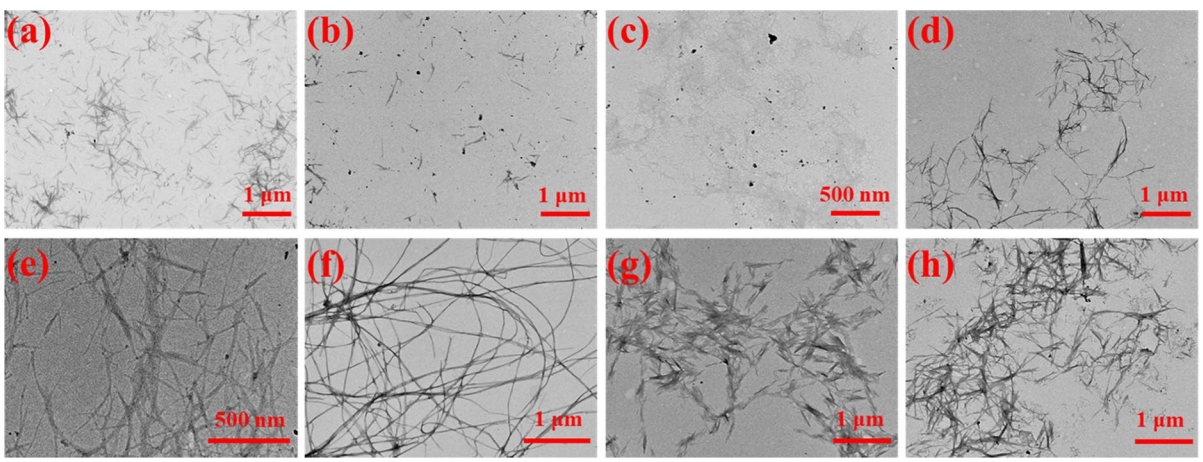

Fig. 1 TEM images of CNCs from different sources: CNCs (**a**), CNC-NH2 (**b**), TEMPO-CNCs (**c**), CNCs-M (**d**), CN-Ls (**e**), B-CNCs (**f**), CN-Ws (**g**) and CN-Fs (**h**)

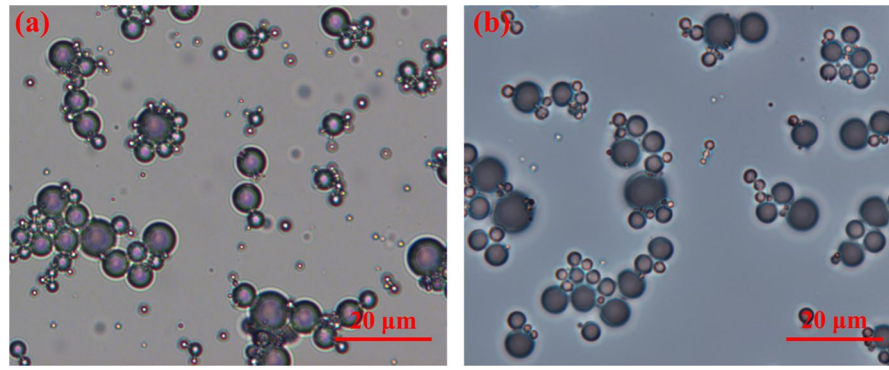

Fig. 2 Morphological images of SonoVue (**a**) and SonoVue@CNC MBs (**b**) taken by IFM (100×). The scale bar is 20 μm. The CNCs used here were obtained from a freeze-dried powder of rod-like CNCs (CAS No: NONE8013, Product No: C909405)

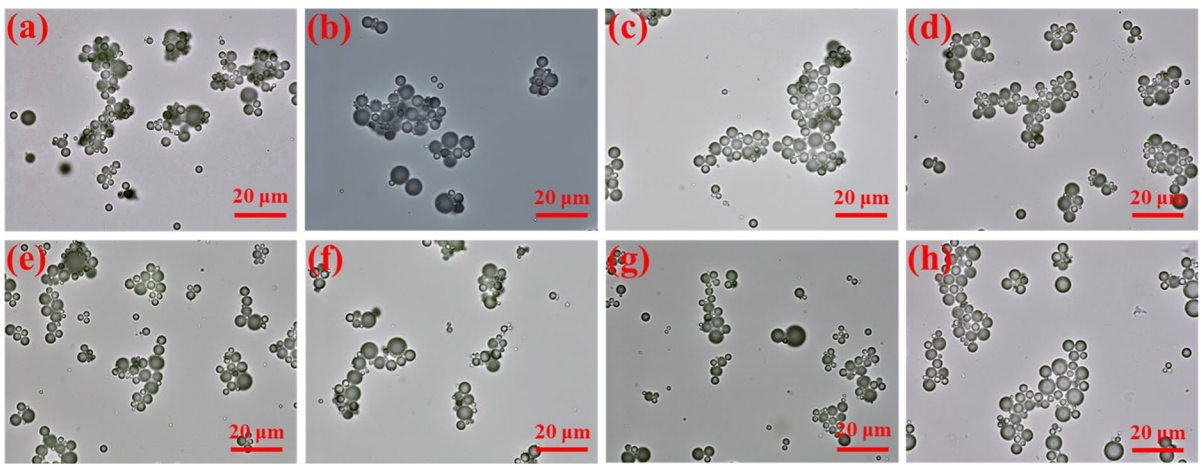

Fig. 3 Morphological images of SonoVue@CNCs (**a**), SonoVue@CNC-NH2 (**b**), SonoVue@TEMPO-CNCs (**c**), SonoVue@CNCs-M (**d**), SonoVue@CN-Ls (**e**), SonoVue@B-CNCs (**f**), SonoVue@CN-Ws (**g**) and SonoVue@CN-Fs (**h**) by IFM (100×)

SonoVue MBs and all CNC-based SonoVue@CNC MBs displayed similar spherical shapes (Fig. 2, 3).

As showed in Fig. 2, both the SonoVue MBs and SonoVue@CNC MBs displayed similar spherical shapes (Fig. 2) with similar uniform granulometric distributions and mean particle sizes (5.50 ± 1.60 μm and 5.08 ± 1.72 μm, respectively), indicating that the introduction of CNCs did not alter the original spherical morphology of SonoVue MBs.

As shown in Fig. 3, all CNC-based MBs (from a to h) maintained similar spherical and uniform particle sizes, confirmed that all types of rod-like CNCs could be incorporated into SonoVue MBs to generate different SonoVue@CNC MBs regardless of their origin.

The morphology of the newly prepared SonoVue@CNC MBs was also analysed via TEM. As shown in Fig. 4a, rod-like CNCs were used to fabricate the SonoVue@CNC MBs.

The TEM results confirmed that commercially available SonoVue MBs were micrometre-sized spherical bubbles, as shown in Fig. 4b. It has been reported that SonoVue MBs comprised the poorly soluble and inactive gas sulphur hexafluoride and polymeric shells, which contained some amphiphilic and surfactant polymeric materials, such as macrogol 4000, DSPC and DPPG-Na. Many salt particles precipitated around the shells, forming a rough membrane structure and a granular shape. Salt particles were observed only in the liquid around the MBs, which confirmed that salt crystallized and separated from the SonoVue@CNC MBs when dried for TEM observation. The precipitation of salt particles from the shells of the MBs resulted in poor shell toughness and rapid collapse in the blood circulation. As shown in Fig. 4c, SonoVue@CNC MBs were also micron-sized spherical MBs. The rod-shaped CNCs

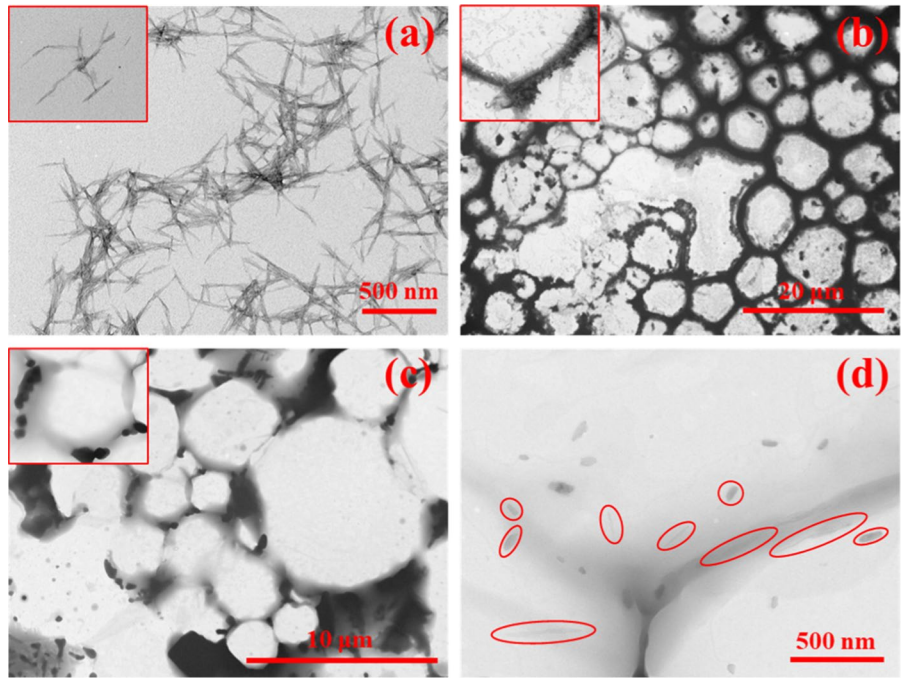

Fig. 4 TEM images of CNCs (**a**), SonoVue (**b**), and SonoVue@CNCs (**c**, **d**). Picture (**d**) is a partial enlargement of SonoVue@CNCs (**c**), and CNCs are circled with red rings. The scale bar is 500 nm. The CNCs used here were obtained from a freeze-dried powder of rod-like CNCs (CAS No: NONE8013, Product No: C909405)

were absorbed or embedded into the polymeric shells to support the SonoVue@CNC MBs. As shown in Fig. 4c, d, the modified shells of the SonoVue@CNC MBs were refined, with fewer salt particles precipitated near the membrane. Negative CNCs displayed great affinity with the amphiphilic and surfactant polymeric materials, such as macrogol 4000, DSPC and DPPG-Na, so the salt was separated and crystallized out along with the CNCs. These results also further confirmed that rod-like shape CNCs can be adsorbed onto SonoVue MBs resulting in CNC-based MBs, thereby forming a preferably refined and tougher shell structure and stabilizing the modified MB shells.

Additionally, all seven other kinds of SonoVue@CNC MBs, e.g., SonoVue@CNC-NH_2 (a), SonoVue@ CNCs-M (b), SonoVue@CNC-Ls (c), SonoVue@B-CNCs (d), SonoVue@CN-Ws (e) and SonoVue@CN-Fs (f), were observed by TEM, and the results are shown in Fig. S6. As shown in Fig. S6, all of the CNC-based MBs maintained a spherical shape and uniform particle size similar to that of SonoVue MBs, which was consistent with the IFM results in Fig. 3. The CNC-based MBs remained stable regardless of the origin, batch or surface charge of the CNCs. Thus, we found that rod-like CNCs from different sources and with different aspect ratios and zeta potentials can all be used to generate SonoVue@CNC MBs. Altogether, CNCs were compatible with SonoVue MBs and absorbed onto the SonoVue MB shells, resulting in new kinds of SonoVue@CNC MBs that maintained a uniform particle size and spherical shape.

Physicochemical properties of SonoVue@CNC MBs

Additionally, the zeta potentials of SonoVue@CNC MBs were seriatim studied. The zeta potentials of SonoVue, CNCs and SonoVue@CNCs were -47.36 ± 0.55 mV, -43.10 ± 1.05 mV and -82.36 ± 3.81 mV, respectively. The zeta potentials of the seven other SonoVue@CNC MBs modified with CNCs from different origins or surface functional groups (CNC-NH_2, TEMPO-CNCs, CNCs-M, CN-Ls, B-CNCs, CN-Ws, and CN-Fs) were also measured. All eight types of CNC samples and the corresponding SonoVue@CNC MBs were negatively charged, as shown in Figs. S1–2, which could help increase their circulation time in vivo. The absolute values of the zeta potentials of both the plain MB and CNC samples and the corresponding SonoVue@CNC MBs were much higher than 30 mV, indicating that these compounds were very stable.

Moreover, the DSC-TGA results showed that the CNCs could maintain their rod-like shape and

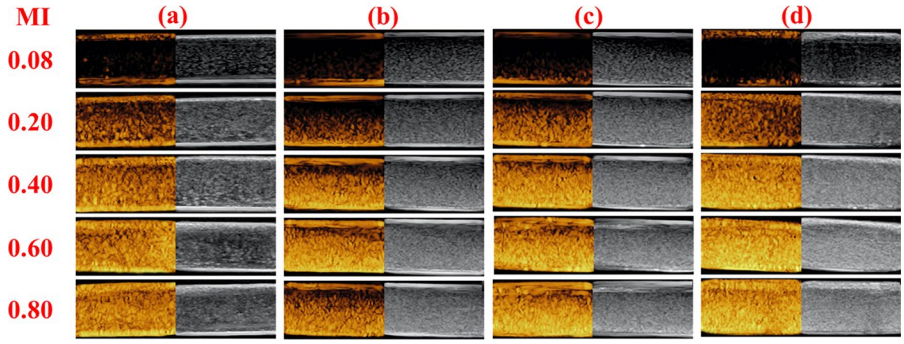

Fig. 5 CEUS (left) and B-mode US (right) images acquired with different MIs in vitro of (**a**) SonoVue, and (**b**–**d**) SonoVue@CNCs with different concentrations of CNCs (12.5 mg/mL, 25 mg/mL and 50 mg/mL, respectively). The picture brightness simply corresponded to the UCA-promoted improvement of US imaging. When the MI was above 0.2, (**d**) the SonoVue@CNCs displayed the biggest enhancement in US imaging under CEUS mode. A HI VISION Ascendus US diagnostic system (HITACHI, Japan) equipped with an EUP-L74M Linear array transducer (5–13 MHz) was used, while the parameters of CEUS were FR (frame rate): 15, BG (B Gain): 15, DR (Dynamic Range): 65, L74M (Ultrasonic probe model) and dCHI-W-P (contrast harmonic imaging depth contrast harmonic imaging), and the experimental parameters for B mode were BG (B Gain): 15, DR (Dynamic Range): 70, and FI (Fundamental imaging)

maintain stable physicochemical properties at 100 °C, as shown in Figs. S3–4. So, the SonoVue@CNC MBs would be stable in the body. These results confirmed that SonoVue@CNC MBs could tolerate a higher MI of US irradiation than SonoVue MBs. In addition, drug-loaded CNCs can be used to construct drug-loaded SonoVue@CNC MBs, as shown in Fig. S5. The drug-loaded SonoVue@CNC MBs will be studied next as US-based cancer theranostic systems, which would expand the biomedical application range of CNCs in the near future. Altogether, SonoVue@CNC MBs could be generated from CNCs and SonoVue MBs, and these methods could be used for all kinds of CNCs.

In vitro *ultrasound imaging of SonoVue@CNC MBs*

An EPIQ7 US diagnostic system (Philips, USA) was used to evaluate the enhancements in US imaging and MI tolerance for SonoVue@CNC MBs in vitro. For qualitative analysis, as shown in Fig. 5 and Fig. S7, the B-mode US and CEUS mode images showed increased brightness as MI increased, regardless of whether SonoVue MBs (a) or SonoVue@CNC (b, c and d) MBs with different concentrations of CNCs were used. Compared to those of the SonoVue group (a), the pictures in the SonoVue@CNC groups (b, a and d) were better visualized, the images were more precise, and the echo intensity increased in both

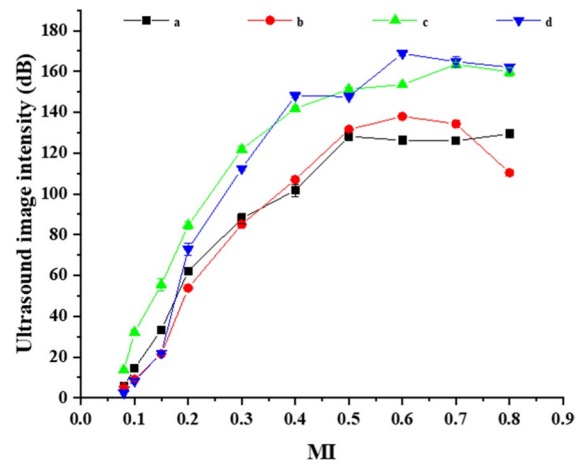

Fig. 6 Quantitative analysis of the mean echo intensity in the drawn ROIs achieved with SonoVue and SonoVue@CNC MBs and different MIs in vitro: (**a**) SonoVue MBs; and (**b**–**d**) SonoVue@CNC MBs with different CNC concentrations (12.5 mg/mL, 25 mg/mL and 50 mg/mL, respectively). The equivalent concentration of SonoVue MBs was 5 mg/mL. The echo intensity in the region of interest (ROI), which was a circle with a diameter of 1.0 cm, was quantitatively analysed by the data analysis software QLAB10

B-mode US and CEUS. This result was especially true when the MI was higher than 0.40. Since CNCs have been used as delivery platforms in drug delivery system, CNC-based SonoVue@CNC MBs indicated broader applications than that of the commercially

available SonoVue. CNC-based MBs can be used to realize US theranostic methods.

As the CNC concentration increased, the image enhancement with the SonoVue@CNC MBs significantly improved. Group (d) SonoVue@CNC, whose CNC concentration was 50 mg/mL, showed the highest image enhancement of all three SonoVue@CNC groups. For quantitative analysis, as shown in Fig. 6 and Fig. S9, the echo intensity of SonoVue@CNC MB groups increased with CNC concentrations under the same MI. Specifically, when the MI value was above 0.30 and the CNC concentration was 12.5 mg/mL, the echo intensity of the SonoVue@CNC group was consistently higher than that of the SonoVue MBs at the same MI. When the CNC concentration was 25 mg/mL, the echo intensity of the SonoVue@CNC group was consistently higher than that of the SonoVue group at the same MI. When the MI value was above 0.15 and the CNC concentration was 50 mg/mL, the echo intensity of the SonoVue@CNC group was also higher than that of SonoVue MBs at the same MI. Among the three CNC concentrations, the best image enhancement was achieved at 25 mg/mL. These findings suggest that CNCs increased the acoustic impedance of SonoVue@CNCs, thereby optimizing the image enhancement. Thus, the CNC concentration regulated the quality of CEUS images in the SonoVue@CNC MB groups in vitro. As previously reported, solid UCAs promote higher US echo intensity and better enhancement in US imaging than the liquid ones under the same conditions. The US imaging enhancement was correlated with the

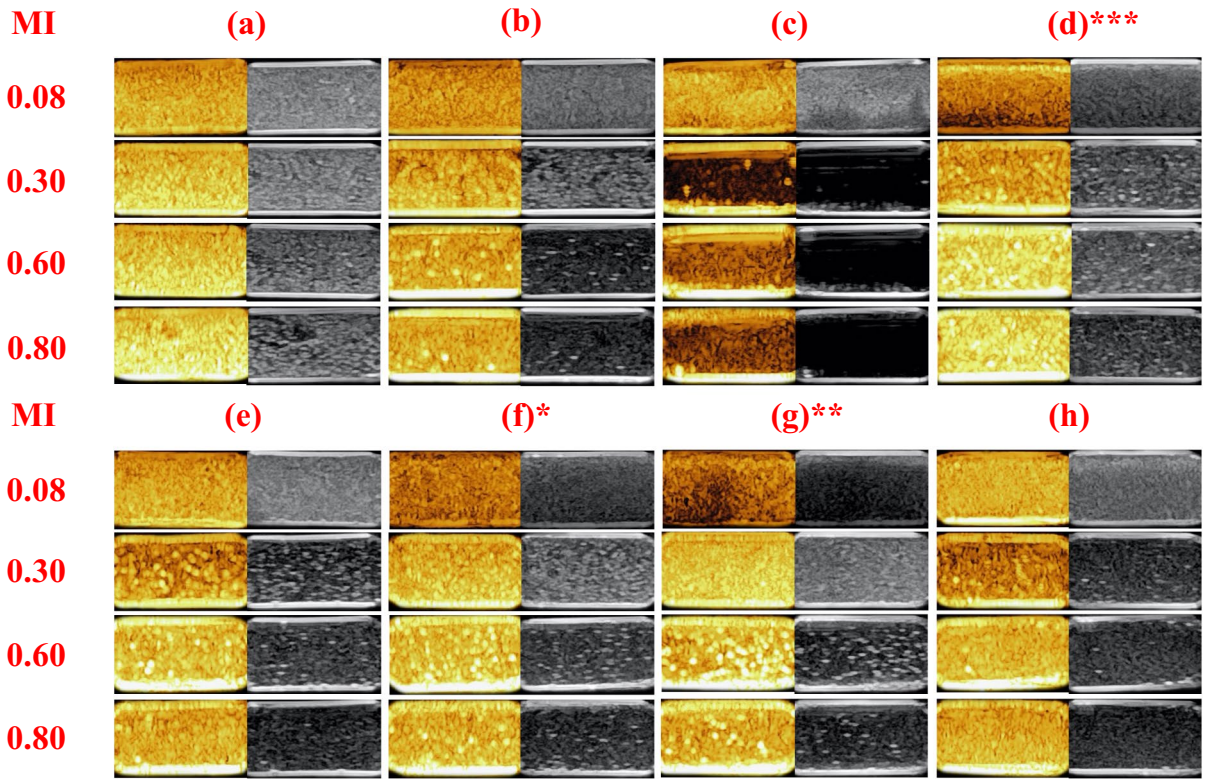

Fig. 7 CEUS and B-mode US images acquired with CNC-based MBs in vitro at different MIs: SonoVue@CNCs (**a**), SonoVue@CNC-NH_2 (**b**), SonoVue@ TEMPO-CNCs (**c**), SonoVue@ CNCs-M (**d**), SonoVue@CNC-Ls (**e**), SonoVue@B-CNCs (**f**), SonoVue@CN-Ws (**g**) and SonoVue@CN-Fs (**h**). ***, **, and * indicate that the enhancement of US imaging was the best, better, and good, respectively, among all eight studied groups. The equivalent concentrations of CNCs and SonoVue solution were 6.4 mg/mL and 5 mg/mL, respectively. A HI VISION Ascendus US diagnostic system (HITACHI, Japan) equipped with an EUP-L74M Linear array transducer (5–13 MHz) was used, while the parameters of CEUS were FR: 15, BG: 15, DR: 65, L74M and dCHI-W-P, and the experimental parameters for B mode were BG: 15, DR: 70, and FI

solid particle concentration. X-ray diffraction results displayed the four main peaks in cellulose I pattern (French 2014; Sun et al. 2018; Ling et al. 2019a, b). The CNCs were observed as nanocrystalline solid particles, as shown in supporting information Fig. S8. Therefore, CNC-modified MBs tolerated a higher MI than MBs alone. CNC-based MBs could be used in US diagnosis for miscellaneous diseases where a high MI is needed.

CEUS and B-mode US images with CNC-based MBs were acquired at different MIs in vitro and carefully observed. All eight types of CNC-based MBs, SonoVue@CNCs (a), SonoVue@CNC-NH_2 (b), SonoVue@ TEMPO-CNCs (c), SonoVue@ CNCs-M (d), SonoVue@CNC-Ls (e), SonoVue@B-CNCs (f), SonoVue@CN-Ws (g), and SonoVue@CN-Fs (h), led to better enhancement on CEUS images acquired with different MI values (0.08, 0.30, 0.60, 0.80), as shown in Fig. 7. Moreover, the enhancement increased with increasing MI. When the MI value was 0.6, all eight CNC-based MBs achieved the best enhancement on both B-mode US and CEUS in vitro. Usually, a high MI (0.6 or higher) was used for the inorganic solid-based UCAs. The excellent properties of solid-based UCAs included a high echo intensity and high MI tolerance. But there are currently no commercially available solid UCAs because their applications are greatly limited by their small size, concentrations and biosafety. All eight types of CNC-modified MBs showed improved MI tolerance and resistance compared to SonoVue MBs. Therefore, CNC-modified SonoVue MBs could maintain their microscale size and enhance their MI tolerance, resulting in improved US images in vitro.

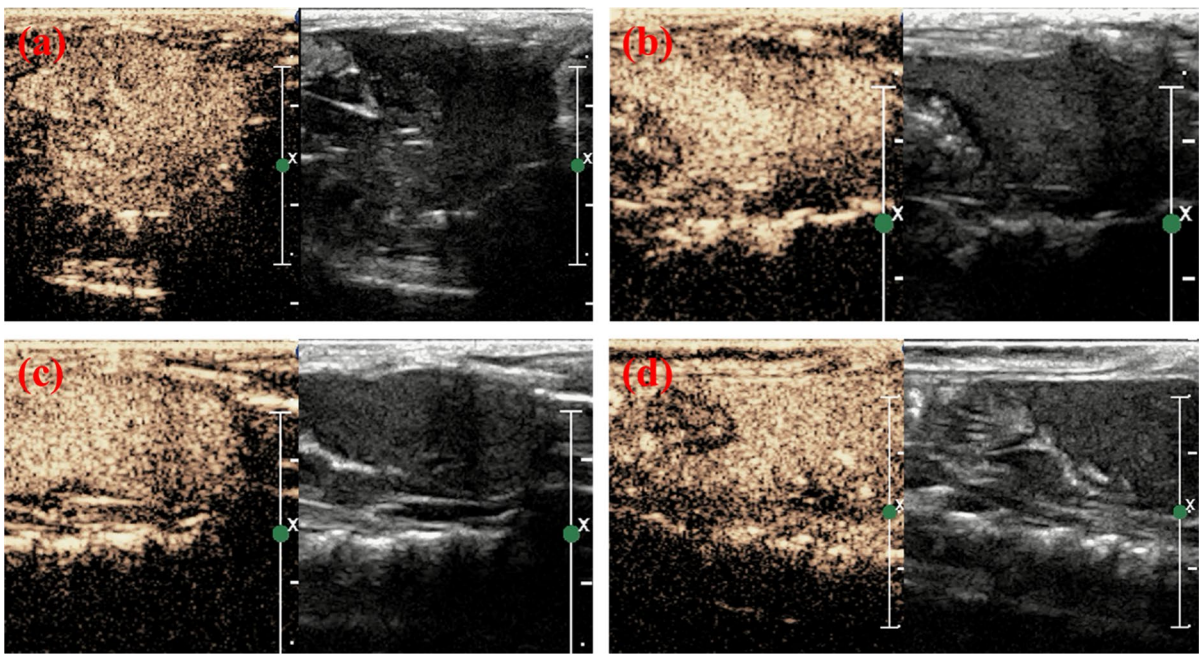

Fig. 8 CEUS and B-mode US images of SD mouse livers acquired 10 s after an intravenous injection of SonoVue MBs (**a**) and SonoVue@CNC MBs (**b**–**d**) through the tail with an MI value of 0.19. The rod-like CNC (CAS No: NONE8013, Product No: C909405) concentrations in SonoVue@CNC MBs were 6.4 mg/mL (**b**), 13.2 mg/mL (**c**) and 26 mg/mL (**d**). The equivalent SonoVue concentration was 5 mg/mL. The green dots and "X" in each image indicate the focused position, with parameters of a depth of 3.5 cm and a focus of 1.5 cm. An EPIQ7 US diagnostic system (Philips, USA) equipped with a L12-5 Linear array transducer (5–12 MHz) was used, while the parameters of CEUS were L12-5 (Ultrasonic probe model), 10 Hz (probe frequency), RS (resolution mode), Contrast 54% (Contrast Gain 54%), C53 (Compress 53), Gen (Generation), MI0.19 L (Low MI), and MI0.24 R (Flsh MI), and the experimental parameters for B mode were Tissue 83% (Tissue Gain 83%), C56 (Compress 56), and Gen (Generation)

Enhanced ultrasound imaging with SonoVue@CNC MBs in vivo

SD mice were used to evaluate the SonoVue@CNCs MB-based enhancement in US imaging using SonoVue as the control group and B-mode as the control mode. As shown in Fig. 8, the liver could be roughly observed on CEUS images using SonoVue (a) or rod-like CNC (CAS No: NONE8013, Product No: C909405)-based SonoVue@CNC MBs with different CNC concentrations (b, c, and d). The blood vessels could be visualized, and detailed information on the liver could be obtained. Compared with the B-mode US images, the CEUS images with SonoVue MBs and SonoVue@CNC MBs both showed higher brightness and clearer blood vessels and related physiological structures in the livers. The image brightness and echo intensity increased as the CNC concentration of the SonoVue@CNCs increased. The inner structure, including tiny blood vessels and any tissue texture, of the liver was relatively obscured in the SonoVue group, while the structures and details could be visualized more clearly in the SonoVue@CNC groups. Regarding CEUS images, the colour in the CEUS images changed from dark yellow to white, indicating that the brightness was much higher in the SonoVue@CNC groups than in the SonoVue group. Among the three SonoVue@CNC groups, a CNC concentration of 6.4 mg/mL resulted in the greatest enhancement in the CEUS images. These results are in accordance with the qualitative and quantitative analysis of echo intensity in Fig. S9 and Fig. 6, which confirmed that higher CNC concentrations in SonoVue@CNC MBs promoted greater enhancements in CEUS images. Altogether, enhanced US images of SD mouse livers were achieved using both SonoVue and SonoVue@CNC MBs, and the enhancement in CEUS was better than that in B-mode US. For both CEUS and B-mode US, the SonoVue@CNC MBs led to a better enhancement than the SonoVue MBs. Because of the characteristics of CNCs that impart strong sound wave propagation and echo intensity, the SonoVue@CNC MBs promoted enhanced US imaging and MI tolerance, which makes it suitable for the diagnosis of difficult and complicated diseases that may cause elongated US irradiation times and require improved US imaging.

The SD mouse kidneys were roughly observed on B-mode US and CEUS mode using SonoVue MBs and SonoVue@CNC MBs, as shown in Fig. 9. The images obtained using the other seven types of SonoVue@CNC MBs are shown in Fig. S10. As shown in Fig. 9, SonoVue@CNC MBs could enhance the clarity of the kidneys on US relative to the surrounding tissues. The enhancement differed when the CNC concentrations of SonoVue@CNC MBs changed. When the CNC concentration was 26 mg/mL, SonoVue@CNC MBs resulted in better enhanced US images than all the other SonoVue@CNC MBs with a different CNC concentration. Under B-mode US, the inner structures of the kidney could not be clearly visualized. The CEUS images of the kidney displayed the highest brightness 5 s after the injection of SonoVue MBs with an echo intensity of 23.51 ± 1.44 dB. Then, the enhancement began to decrease at 10 s, and the kidney became obscured. In comparison, the brightness was the highest 5 s after the injection of SonoVue@CNC MBs with echo intensities of 30.07 ± 0.96 dB, 31.82 ± 3.24 dB, and 35.29 ± 1.12 dB, and the kidney morphology and inner structures were clearly visualized. Even 10 s after the injection, the image brightness was not significantly attenuated, and the kidney morphology was still clearly visible. The echo intensity and image clarity at 5 s and 10 s after the injection of SonoVue@CNC MBs with different CNC concentrations were better than those after the injection of SonoVue MBs. This phenomenon was especially true at a CNC concentration of 26 mg/mL, at which the best image was obtained.

Moreover, seven other CNCs were used to generate CNC-based SonoVue@CNC MBs. Newly generated CNC-based MBs displayed similar enhancement for US images in vitro (Fig. 7) and in vivo (Fig. S11). All CNC-based SonoVue@CNC MBs improved US imaging when the MI was lower than 0.6. When the MI value was 0.60, the enhanced US imaging showed some differences among the eight kinds of SonoVue@CNC MBs in vitro. The eight kinds of SonoVue@CNC MBs were all spherical with similar particle sizes, as shown in Fig. 2, indicating a similar tolerance and US image enhancement in vitro (Fig. 7) and in vivo (Figs. S11–12). The enhancement in US imaging caused by the SonoVue@CNC MBs was mainly induced by the incorporated CNC particles. So, the length and width of CNCs can affect their echo intensity, resulting in differences in US imaging.

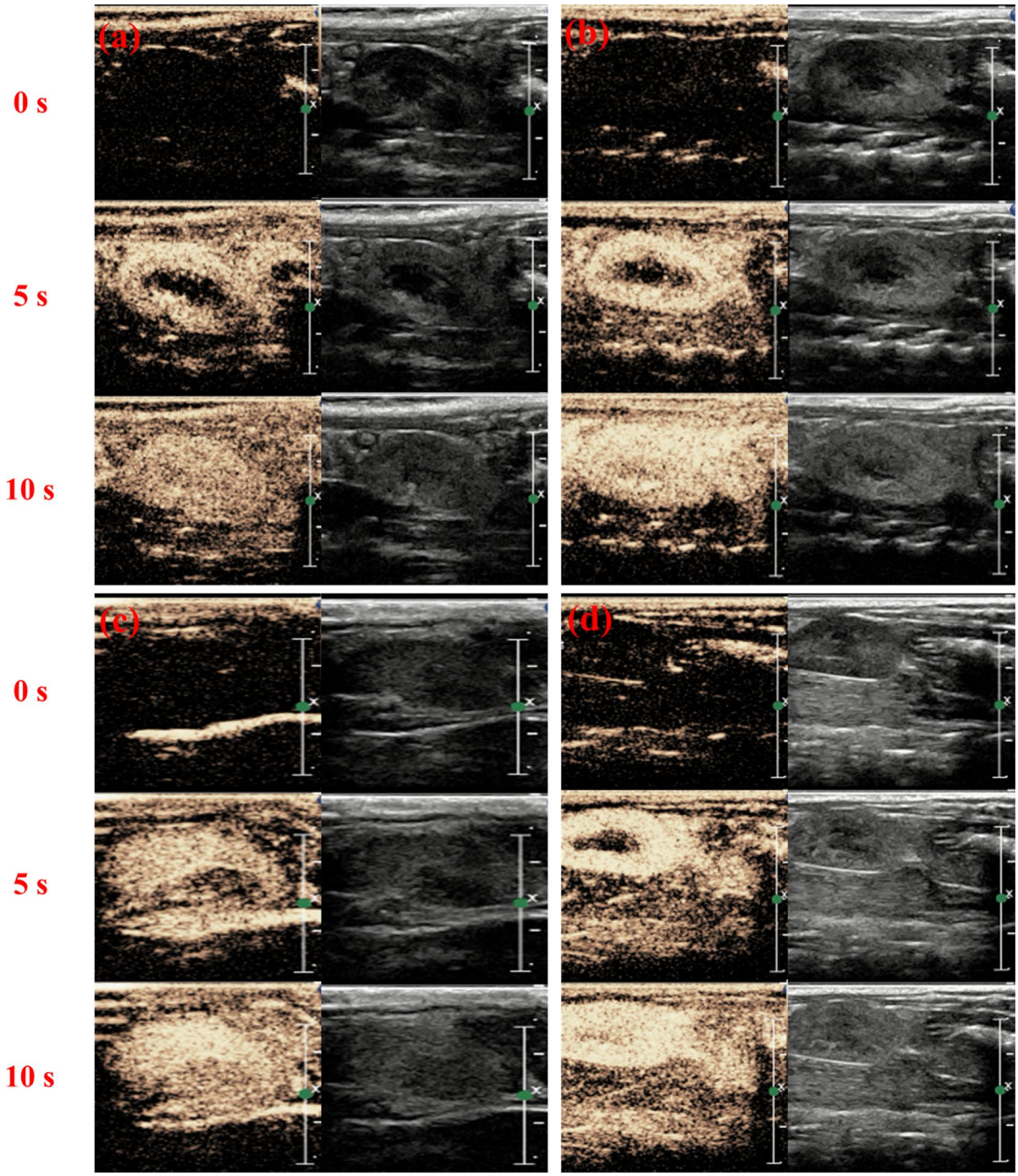

Fig. 9 CEUS and B-mode US images of SD mouse kidneys acquired within 10 s after an intravenous injection of SonoVue MBs (**a**) and SonoVue@CNC MBs (**b–d**) through the tail vein with an MI of 0.19. The CNC concentrations in the SonoVue@CNC MB groups were 6.4 mg/mL (**b**), 13.2 mg/mL (**c**) and 26 mg/mL (**d**). The equivalent SonoVue concentration was 5 mg/mL. The green dots and "X" in each image indicate the focused position, with parameters of a depth of 3.5 cm and a focus of 1.5 cm. An EPIQ7 US diagnostic system (Philips, USA) equipped with an L12-5 Linear array transducer (5–12 MHz) was used, while the parameters of CEUS were L12-5, 10 Hz, RS, Contrast 54%, C53, Gen, MI0.19 L, and MI 0.24 R, and the experimental parameters for B mode were Tissue 83%, C56, and Gen

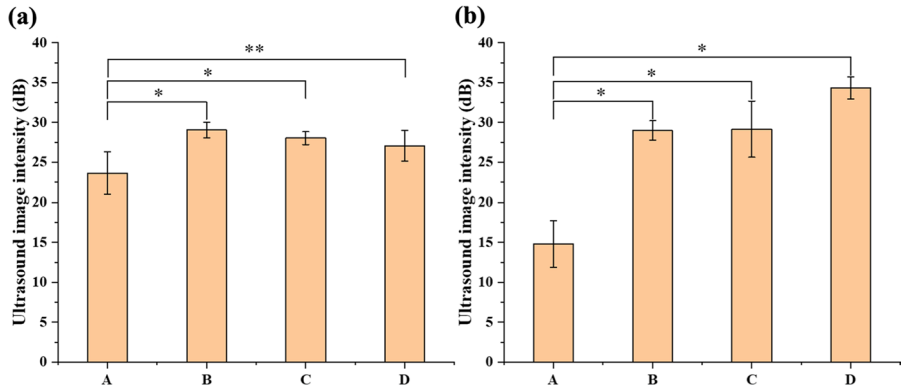

Fig. 10 Quantitative analysis of the echo intensity in CEUS images of SD mice. The ROI values of the livers (**a**) and kidneys (**b**) were obtained 10 s after the injections of SonoVue MBs (A) and SonoVue@CNC MBs (B, C and D). The CNC concentrations in groups B, C and D were 6.4 mg/mL, 13.2 mg/mL and 26 mg/mL, respectively. The equivalent SonoVue MB concentration was 5 mg/mL. $*P<0.05$, $**P<0.01$. The echo intensity in the region of interest (ROI), which was a circle with a diameter of 1.0 cm, was quantitatively analysed by the data analysis software QLAB10

The echo intensity was quantified on US images obtained with all eight types of CNC-modified SonoVue MBs, and the data are shown in In Fig. 10 and Fig. S13. The echo intensities of SD mouse livers with SonoVue MBs (group A) and SonoVue@CNCs (groups B, C and D) were 23.64 ± 1.68 dB, 29.05 ± 1.98 dB, 28.04 ± 1.82 dB, and 27.06 ± 1.95 dB, respectively (Fig. 10a), showing that SonoVue@CNC MBs exhibited consistently higher echo intensity in SD mouse livers than the SonoVue MBs did. On the liver images, the highest echo intensity and best image enhancement were obtained in all the groups when the CNC concentration was 6.4 mg/mL. The echo intensities of SD mouse kidneys (b) in groups A, B, C and D were 14.81 ± 1.91 dB, 28.98 ± 1.23 dB, 29.15 ± 1.52 dB, and 34.33 ± 1.41 dB, respectively, revealing that SonoVue@CNC MBs similarly exhibited consistently higher echo intensity in SD mouse kidneys than the SonoVue MBs did. On the kidney images, the highest echo intensity and best image enhancement were obtained in all groups when the CNC concentration was 26 mg/mL. Therefore, CNC-based SonoVue@CNC MBs created higher echo intensities than SonoVue MBs, which was further verified using the seven CNC-modified MBs

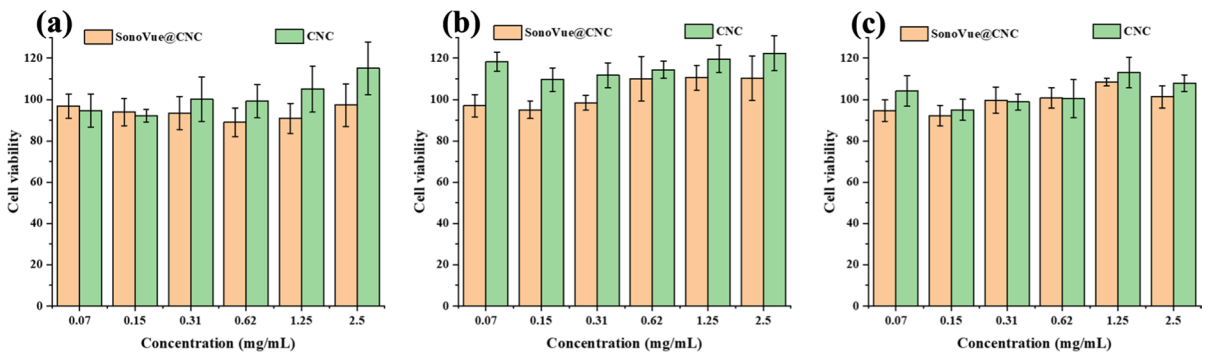

Fig. 11 Cell viability of MCF-10A cells co-incubated with CNCs and SonoVue@CNCs for 6 h (**a**), 12 h (**b**), and 24 h (**c**). Data are presented as the mean ± SD. The equivalent CNC concentrations were 0.07 mg/mL, 0.15 mg/mL, 0.31 mg/mL, 0.62 mg/mL, 1.25 mg/mL, and 2.5 mg/mL. The mean and SD are shown. The equivalent SonoVue MB concentration was 5 mg/mL. PBS and MCF-10A cells coincubated in complete medium were used as the blank and control groups

for in vivo and in vitro imaging, as shown in Fig. 7 and Figs. S11–12. The absorption of CNC nanoparticles with a large aspect ratio could increase the shell thickness, hardness and specific surface area of MBs, resulting in enhanced echo intensity. Altogether, CNCs obtained from different batches (Figs. S14–16), with a different origin and with the same rod-like shape (Fig. 4) and negative charge (Fig. S2) could all improve the US tolerance of SonoVue@CNC MBs while maintaining excellent enhancement of US imaging in vitro and in vivo (Fig. 7 and Figs. S10–12). Therefore, the CNC-modified MBs would have greater stability and broader applications than SonoVue MBs.

Toxic effects of SonoVue@CNC MBs against MCF-10A cells

Cytotoxicity and biocompatibility were preliminarily evaluated by the CCK-8 assay. As shown in Fig. 11, the cell viability for almost all cell groups was higher than 90% when MCF-10A cells were coincubated with CNCs and SonoVue@CNCs for 6 h (a), 12 h (b), and 24 h (c). Therefore, both CNCs and SonoVue@CNC MBs were safe against MCF-10A cells. Moreover, the proliferation of cells coincubated with both SonoVue@CNCs and CNCs was independent of the CNC dose. Therefore, when the CNC concentration was lower than 2.5 mg/mL, the CNCs did not exhibit significant cytotoxicity, which is in agreement with previously reported results (Ventura et al. 2020). There were no significant differences in the cell survival rates between the SonoVue@CNC and CNC groups ($P > 0.05$). Therefore, neither SonoVue@CNCs nor CNCs were cytotoxic, and both displayed acceptable biocompatibilities.

Although this study confirms that SonoVue@CNC MBs can be fabricated via self-assembly technology, which was also evaluated in vitro and in vivo for US imaging, there are still some scientific limitations and problems to be resolved. For instance, the combined efficiency of CNCs and SonoVue MBs, the precise changes in shell thickness and the biosecurity in vivo all need to be more clearly elucidated to expand the range of biomedical applications of CNCs and SonoVue MBs.

Conclusions

SonoVue@CNC MBs were successfully prepared by dispersing CNCs into SonoVue MBs. The rod-like CNCs were adsorbed onto the polymeric MB shells, resulting in enhanced echo intensities, MI tolerances and increased surface areas for the SonoVue@CNC MBs. Therefore, SonoVue@CNC MBs demonstrated better US image enhancement both in vitro and in vivo than SonoVue MBs. Chemotherapeutic agents and targeted molecules will be loaded in SonoVue@CNC MBs via CNC-based self-assembly in the near future by our group to develop new kinds of UCAs and UCA-based targeted theranostic systems.

Acknowledgments This study was supported by the National Key Research and Development Program of China (Grant No. 2018YFC0114606), the joint and collaborative project of Henan Medical Science and technology research program (LHGJ20210020) and the Project of Basic Research Fund of Henan Provincial Institute of Medical and Pharmacological Sciences (2022BP0110).

Author contributions All authors contributed to the study conception and design. Material preparation, data collection and analysis were performed by YW, NL, YW and BZ. Conceptualization: NL, YW and SD; Methodology: NL; Formal analysis and investigation: YW; Writing—original draft preparation: YW, NL; Writing—review and editing: YW; Funding acquisition: LZ; Resources: SR and YZ; Supervision: LZ, The first draft of the manuscript was written by YW and all authors commented on previous versions of the manuscript. All authors read and approved the final manuscript. All data included in this study will be made available upon request by the corresponding authors.

Declarations

Competing interests The authors have no relevant financial or non-financial interests to disclose.

References

Albanese A, Tang PS, Chan WCW (2012) The effect of nanoparticle size, shape, and surface chemistry on biological systems. Annu Rev Biomed Eng 14:1–16. https://doi.org/10.1146/annurev-bioeng-071811-150124

Ates B, Koytepe S, Ulu A, Gurses C, Thakur VK (2020) Chemistry, structures, and advanced applications of nanocomposites from biorenewable resources. Chem Rev 120:9304–9362. https://doi.org/10.1021/acs.chemrev.9b00553

Bez M, Foiret J, Shapiro G, Pelled G, Ferrara KW, Gazit D (2019) Nonviral ultrasound-mediated gene delivery in small and large animal models. Nat Protoc 14:1015–1026. https://doi.org/10.1038/s41596-019-0125-y

Chen L, Berry RM, Tam KC (2014) Synthesis of β-Cyclodextrin-modified cellulose nanocrystals (CNCs)@Fe3O4@SiO2 superparamagnetic nanorods. ACS Sustain Chem Eng 2:951–958. https://doi.org/10.1021/sc400540f

Chithrani BD, Chan WCW (2007) Elucidating the mechanism of cellular uptake and removal of protein-coated gold nanoparticles of different sizes and shapes. Nano Lett 7:1542–1550. https://doi.org/10.1021/nl070363y

Cintrón MS, Johnson GP, French AD (2011) Young's modulus calculations for cellulose Iβ by MM3 and quantum mechanics. Cellulose 18:505–516. https://doi.org/10.1007/s10570-011-9507-1

French AD (2014) Idealized powder diffraction patterns for cellulose polymorphs. Cellulose 21:885–896. https://doi.org/10.1007/s10570-013-0030-4

French AD, Santiago Cintrón M (2013) Cellulose polymorphy, crystallite size, and the Segal Crystallinity Index. Cellulose 20:583–588. https://doi.org/10.1007/s10570-012-9833-y

Gratton SEA, Ropp PA, Pohlhaus PD, Luft JC, Madden VJ, Napier ME, DeSimone JM (2008) The effect of particle design on cellular internalization pathways. Proc Natl Acad Sci 105:11613–11618. https://doi.org/10.1073/pnas.0801763105

Guo J, Guo X, Wang S, Yin Y (2016) Effects of ultrasonic treatment during acid hydrolysis on the yield, particle size and structure of cellulose nanocrystals. Carbohydr Polym 135:248–255. https://doi.org/10.1016/j.carbpol.2015.08.068

Imlimthan S, Otaru S, Keinänen O, Correia A, Lintinen K, Santos HA, Airaksinen AJ, Kostiainen MA, Sarparanta M (2019) Radiolabeled molecular imaging probes for the in vivo evaluation of cellulose nanocrystals for biomedical applications. Biomacromol 20:674–683. https://doi.org/10.1021/acs.biomac.8b01313

Jorfi M, Roberts MN, Foster EJ, Weder C (2013) Physiologically responsive, mechanically adaptive bio-nanocomposites for biomedical applications. ACS Appl Mater Interfaces 5:1517–1526. https://doi.org/10.1021/am303160j

Li J, Wang Y, Zhang L, Xu Z, Dai H, Wu W (2019a) Nanocellulose/gelatin composite cryogels for controlled drug release. ACS Sustain Chem Eng 7:6381–6389. https://doi.org/10.1021/acssuschemeng.9b00161

Li N, Lu W, Yu J, Xiao Y, Liu S, Gan L, Huang J (2018) Rod-like cellulose nanocrystal/cis-aconityl-doxorubicin prodrug: a fluorescence-visible drug delivery system with enhanced cellular uptake and intracellular drug controlled release. Mater Sci Eng C 91:179–189. https://doi.org/10.1016/j.msec.2018.04.099

Li N, Wang Y, Guo Y, Ji Z, Zhang Z, Yu J, Zhang L (2021) Surface modified cellulose nanocrystalline hybrids actualizing efficient and precise delivery of doxorubicin into nucleus with: in vitro and in vivo evaluation. J Appl Polym Sci 138:1–12. https://doi.org/10.1002/app.51536

Li N, Zhang H, Xiao Y, Huang Y, Xu M, You D, Lu W, Yu J (2019b) Fabrication of cellulose-nanocrystal-based folate targeted nanomedicine via layer-by-layer assembly with lysosomal pH-controlled drug release into the nucleus. Biomacromol 20:937–948. https://doi.org/10.1021/acs.biomac.8b01556

Lin N, Dufresne A (2014) Nanocellulose in biomedicine: current status and future prospect. Eur Polym J 59:302–325. https://doi.org/10.1016/j.eurpolymj.2014.07.025

Lindner JR (2004) Microbubbles in medical imaging: current applications and future directions. Nat Rev Drug Discov 3:527–532. https://doi.org/10.1038/nrd1417

Ling Z, Edwards JV, Guo Z, Prevost NT, Nam S, Wu Q, French AD, Xu F (2019a) Structural variations of cotton cellulose nanocrystals from deep eutectic solvent treatment: micro and nano scale. Cellulose 26:861–876. https://doi.org/10.1007/s10570-018-2092-9

Ling Z, Wang T, Makarem M, Santiago Cintrón M, Cheng HN, Kang X, Bacher M, Potthast A, Rosenau T, King H, Delhom CD, Nam S, Vincent Edwards J, Kim SH, Xu F, French AD (2019b) Effects of ball milling on the structure of cotton cellulose. Cellulose 26:305–328. https://doi.org/10.1007/s10570-018-02230-x

Liu K, Nasrallah J, Chen L, Huang L, Ni Y (2015) Preparation of CNC-dispersed Fe 3 O 4 nanoparticles and their application in conductive paper. Carbohydr Polym 126:175–178. https://doi.org/10.1016/j.carbpol.2015.03.009

Lu P, Lo HY (2010) Preparation and properties of cellulose nanocrystals: rods, spheres, and network. Carbohydr Polym 82:329–336. https://doi.org/10.1016/j.carbpol.2010.04.073

Pereira PHF, Ornaghi Júnior HL, Coutinho LV, Duchemin B, Cioffi MOH (2020) Obtaining cellulose nanocrystals from pineapple crown fibers by free-chlorite hydrolysis with sulfuric acid: physical, chemical and structural characterization. Cellulose 27:5745–5756. https://doi.org/10.1007/s10570-020-03179-6

Seo JH, Lee SY, Hwang CR, Yang M, Lee J, Lee SH, Cho HJ (2020) Multi-layered cellulose nanocrystal system for CD44 receptor-positive tumor-targeted anticancer drug delivery. Int J Biol Macromol 162:798–809. https://doi.org/10.1016/j.ijbiomac.2020.06.193

Sheikhi A, Hayashi J, Eichenbaum J, Gutin M, Kuntjoro N (2019) Recent advances in nanoengineering cellulose for cargo delivery. J Control Release 294:53–76. https://doi.org/10.1016/j.jconrel.2018.11.024

Sun X, Mei C, French AD, Lee S, Wang Y, Wu Q (2018) Surface wetting behavior of nanocellulose-based composite films. Cellulose 25:5071–5087. https://doi.org/10.1007/s10570-018-1927-8

Tang J, Sisler J, Grishkewich N, Tam KC (2017) Functionalization of cellulose nanocrystals for advanced applications.

J Colloid Interface Sci 494:397–409. https://doi.org/10.1016/j.jcis.2017.01.077

Thomas RG, Jonnalagadda US, Kwan JJ (2019) Biomedical applications for gas-stabilizing solid cavitation agents. Langmuir 35:10106–10115. https://doi.org/10.1021/acs.langmuir.9b00795

Toy R, Peiris PM, Ghaghada KB, Karathanasis E (2014) Shaping cancer nanomedicine: the effect of particle shape on the in vivo journey of nanoparticles NIH Public Access. Nanomedicine (lond) 9:121–134. https://doi.org/10.2217/nnm.13.191

Trache D, Hussin MH, Haafiz MKM, Thakur VK (2017) Recent progress in cellulose nanocrystals: sources and production. Nanoscale. https://doi.org/10.1039/C6NR09494E

Ventura C, Pinto F, Lourenço AF, Ferreira PJT, Louro H, Silva MJ (2020) On the toxicity of cellulose nanocrystals and nanofibrils in animal and cellular models. Cellulose 27:5509–5544. https://doi.org/10.1007/s10570-020-03176-9

Wang X, Yu X, Wang X, Qi M, Pan J, Wang Q (2019) One-step nanosurface self-assembly of d -peptides renders bubble-free ultrasound theranostics. Nano Lett 19:2251–2258. https://doi.org/10.1021/acs.nanolett.8b04632